Wang, Peng; Li, Zhina; Ni, Hongjian; Liu, Yuandong; Dou, Peng

Article

Experimental study of rock breakage of an interrupted pulsed waterjet

Energy Reports

Provided in Cooperation with:
Elsevier

Suggested Citation: Wang, Peng; Li, Zhina; Ni, Hongjian; Liu, Yuandong; Dou, Peng (2020) : Experimental study of rock breakage of an interrupted pulsed waterjet, Energy Reports, ISSN 2352-4847, Elsevier, Amsterdam, Vol. 6, pp. 713-720, https://doi.org/10.1016/j.egyr.2020.03.018

Energy Reports 6 (2020) 713–720

Contents lists available at ScienceDirect

Energy Reports

journal homepage: www.elsevier.com/locate/egyr

Research paper

Experimental study of rock breakage of an interrupted pulsed waterjet

Peng Wang [a,b], Zhina Li [c,*], Hongjian Ni [a,b], Yuandong Liu [d], Peng Dou [e]

[a] Key Laboratory of Unconventional Oil & Gas Development (China University of Petroleum (East China)), Ministry of Education, Qingdao 266580, China
[b] School of Petroleum Engineering, China University of Petroleum (East China), Qingdao 266580, China
[c] School of Geosciences, China University of Petroleum (East China), Qingdao 266580, China
[d] China petroleum technology and development corporation, Beijing 100028, China
[e] CNOOC China Limited, Tianjin Branch, Tianjin 300459, China

ARTICLE INFO

Article history:
Received 5 January 2020
Received in revised form 18 March 2020
Accepted 19 March 2020
Available online xxxx

Keywords:
Valve spring blocking
Pulsed waterjet
Rock breakage
Structure optimizing

ABSTRACT

Novel valve spring blocking structure for generating pulsed waterjet was proposed, which belonged to interrupted type and purposed using in petroleum drilling. The characteristics and rock breakage performances of the pulsed waterjet were studied through experiments by changing its structural parameters. Results showed that the pulsed waterjet could be generated through the reciprocating motion of stem under the pressure difference and its rock breakage performance was better than continuous jet under the same conditions. The theoretical frequencies were slightly higher than the experimental value due to the ignorance of friction resistance between components and viscous resistance of fluid. The results provided a basis for its applications in petroleum drilling engineering.

1. Introduction

Waterjets have been used for rock breakage for centuries due to the low cutting forces and high efficiency (Farmer and Attewell, 1965; Lu et al., 2015; Momber, 2003). In order to improve the erosion effect of waterjets under lower pressure, several types of waterjets have been developed over the years (Liu et al., 2020), including cavitating waterjet, abrasive waterjet, pulsed waterjet and rotating waterjet. Among them, pulsed waterjet, which a non-continuous jet and composed of a series of discrete water-slugs, can cause huge damage to the surface and interior of the target by generating water hammer effect (Foldyna et al., 2009; Dehkhoda and Hood, 2014; Ghadi et al., 2016; Foldyna et al., 2020), and has a potential use in breaking hard-rock due to its high-power intensity, simple machinery and minimal tool-wear characteristics (Vijaym, 1995).

A well-established rock breakage mechanism using pulsed waterjets is that a water-hammer pressure is applied on the solid–liquid interface when the highly compressed water pulse reaches the rock surface (Bowden and Field, 1964; Heymann, 1970; Lesser and Field, 2003; Rein, 1993; Sahaya Grinspan and Gnanamoorthy, 2010). The pressure difference across the free surface detaches the shock wave from the contact edge and triggers high-velocity lateral jetting, which is two to five times the impact velocity and good for cuttings removing (Bizanti, 1990) and then the pressure on the solid–liquid interface reduces to the stagnation pressure. The cyclic loading induced by the pulsed jets will intensify the fatigue failure of the rock and the surface layer removal. Many researches discussed the influences of the velocity, nozzle diameter, stand-off distance and rock properties on the breakage performances of pulsed waterjet (Dehkhoda et al., 2012; Hood et al., 1990).

The pulsed waterjets can be modulated by several methods, such as compressed, interrupted and excited (Li et al., 2016). The compressed way needs power producer that can generate periodical energy and then the energy is transmitted to the fluid to actuate the fluid erupting at high velocity. The interrupted way includes rotating a disk and reciprocating a piston, and has been successfully applied, whose challenges are the durability and reliability of moving components in harsh working environments (Nebeker, 1987; Xue et al., 2019). The exited way is based on the principle of self-resonating nozzles (Johnson et al., 1982; Li et al., 2016; Liu et al., 2018; Morel, 1979). Magnetostriction and piezoelectric actuators are also used for generating pulsed waterjet (Foldyna et al., 2006, 2004; Riha and Foldyna, 2012). Of these methods, the interrupted pulsed waterjet devices can generate completely interrupted pulses, which may eliminate the water cushion effect and fully utilizes the water hammer pressure in rock breakage, and is simple to implement with good controllability for field applications (Liu et al., 2015).

In this paper, a valve spring blocking modulation tool of pulsed waterjet is proposed (see Fig. 1), which belongs to interrupted type and purposes using in petroleum drilling. The drilling fluid

* Corresponding author.
E-mail address: lizhina00@163.com (Z. Li).

https://doi.org/10.1016/j.egyr.2020.03.018

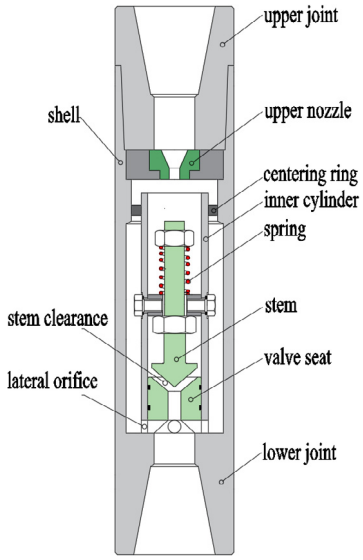

Fig. 1. Structure diagram of the valve spring blocking drilling tool.

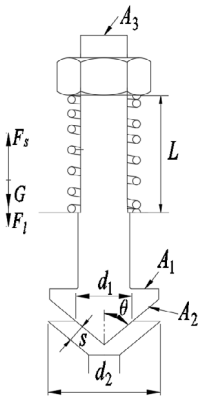

Fig. 2. The force analysis of the stem.

flows through the upper nozzle and enters into the inner cylinder. When the drilling fluid flows through the narrow gap between the stem and valve seat, a pressure difference between the top and bottom of the stem is formed due to Bernoulli effect and pushes the stem moving downwards to compress the spring. The passageway of the drilling fluid will be closed instantaneously once the stem touching the valve seat, and a positive and negative water hammer pressure are formed above and below the stem, respectively. The negative water hammer pressure spreads downward and erupts out of the drill bit nozzle acting on the bottom hole and decreases the bottom hole pressure. Meanwhile, the positive water hammer pressure transmits from the top to the bottom of the stem along the interior of the inner cylinder and the annulus between the inner cylinder and shell, and erupts out of the drill bit nozzle acting on the bottom hole and increases the bottom hole pressure. When the positive water hammer pressure reaches the bottom of the stem the pressure difference between the top and bottom surfaces of the stem is balanced, and then the stem moves upward from the lowest point to the highest point under the action of spring force. The passageway between the stem and valve seat is reopened and the water hammer pressure disappears. The above processes repeat and a pulse jet is generated in succession.

The major work of this paper is composed of the following parts: we first theoretically analyzed the modulation mechanism and characteristics of pulsed jet, then we developed a prototype to study the pulsed characteristics and rock breakage effect of pulsed jet under different operating and structural parameters, and obtained the optimal structure of prototype under laboratory conditions. The research verified the feasibility of proposed valve spring blocking tool and provided basis for the development of related technologies.

2. Modulation mechanism of the pulsed waterjet

When the drilling fluid flows through the annulus between the stem and valve seat, a pressure difference between the upper and lower ends of the stem forms owing to the Bernoulli's effect. The resultant force of the pressure difference, stem gravity and spring force pushes the stem moving advance and return along the stem axis (see Fig. 2). The clearance between the stem and valve seat changes periodically as the stem moving. A positive water hammer pressure and negative water hammer pressure alternate below the valve seat and are transmitted directly to the drill bit nozzles. The working process of the modulation tool can be subdivided into three stages: the stem moving downward stage (i.e. the stem moves downward from the highest point until the clearance between the stem and valve seat becomes zero), the positive water hammer pressure transmitting stage (i.e. the water hammer pressure transmitting from the top to the bottom of the stem along the interior of the inner cylinder and the annulus between the inner cylinder and shell during the flow channel between the stem and valve seat closing) and the stem moving upward stage (i.e. the stem moves upward from the lowest point to the highest point when the pressure difference is balanced).

The forces acting on the stem include the fluid pressure difference $\vec{F}_l$, stem gravity $\vec{G}$ and spring force $\vec{F}_s$. The pressure difference between the top and bottom surface of the stem can be expressed as

$$F_l = \rho_l c A \cdot \Delta v = \rho_l c (A_1 - A_2 + A_3) \cdot \Delta v \tag{1}$$

where F_l is the fluid pressure difference, N; ρ_l is the density of drilling fluid, kg/m^3; c is the pressure wave propagation velocity, m/s; v is the drilling fluid flow velocity at the entrance of valve seat, m/s; A is the effective action area of drilling fluid, m^2; A_1, A_2, A_3 are the action areas of drilling fluid, m^2.

The flow velocity at the entrance of valve seat can be expressed as

$$v = \frac{4Q}{\pi(d_2^2 - d_1^2)} \tag{2}$$

where Q is flow rate, m^3/s; d_1 and d_2 are the diameters of the stem end, m.

According to geometric relation

$$s = \frac{d_2 - d_1}{2} \cos\theta \tag{3}$$

where s is the clearance between stem and valve seat, m; θ is the taper angle of the stem, rad.

The flow velocity at the entrance of valve seat changes to the following form

$$v = \frac{Q}{s\pi} \frac{\cos\theta}{(d_2 - \frac{s}{\cos\theta})} \tag{4}$$

The spring force can be expressed as

$$F_s = k(x + \frac{s}{\sin\theta}) \tag{5}$$

where F_s is the spring force, N; k is the spring stiffness, N/m; x is the initial compression, m.

The following equation can be obtained according to the energy and momentum conservations

$$F_l\frac{s}{\sin\theta}-\frac{1}{2}k(x+\frac{s}{\sin\theta})^2=\frac{1}{2}mv_h^2-mg\frac{s}{\sin\theta} \tag{6}$$

$$(F_l-F_s+G)\,T_1=mv_h \tag{7}$$

where m is mass of the stem mass, kg; v_h is the downward velocity of stem, m/s; T_1 is the time for stem moving downward to the lowest point, s.

Substituting Eqs. (1), (4)–(6) into Eq. (7) we can obtain the turn-off time of the clearance between the stem and valve seat

$$T_1=\frac{\sqrt{2m\left[\rho_l c(A_1-A_2+A_3)\frac{s}{\sin\theta}1\frac{Q}{s\pi}\frac{\cos\theta}{(d_2-\frac{s}{\cos\theta})}-\frac{k}{2}(x+\frac{s}{\sin\theta})^2+mg\frac{s}{\sin\theta}\right]}}{\rho_l c(A_1-A_2+A_3)\frac{Q}{s\pi}\frac{\cos\theta}{(d_2-\frac{s}{\cos\theta})}-k(x+\frac{s}{\sin\theta})+mg} \tag{8}$$

After the stem contacting the valve seat, the high-pressure drilling fluid transmits from the top to the bottom of the stem along the interior of the inner cylinder and the annulus between the inner cylinder and shell to counterweigh the pressure difference acting on the stem. The transmitting time of the pressure wave is

$$T_2=\frac{2L}{\zeta c} \tag{9}$$

where T_2 is the transmitting time of the pressure wave from the top to the bottom of the stem along the interior of the inner cylinder and the annulus between the inner cylinder and shell, s; L is the inner cylinder length, m; ζ is the influence coefficient of external cylinder and adjacent material on the pressure wave.

When the high-pressure wave reaching the bottom of the stem, the pressure difference acting on the stem will be balanced. According to the energy and momentum conservations the following equations can be obtained

$$\frac{1}{2}k(x+\frac{s}{\sin\theta})^2\zeta-mg\frac{s}{\sin\theta}=\frac{1}{2}mv'^2 \tag{10}$$

$$\zeta k(x+\frac{s}{\sin\theta})T_3=mv' \tag{11}$$

where T_3 is the time of stem moving upwards, s; v' is the velocity of stem when it reaches the highest point, m/s.

Combining equations (10) and (11) the time of the stem moving upwards can be obtained

$$T_3=\frac{\sqrt{m\zeta k(x+\frac{s}{\sin\theta})^2-\frac{2m^2gs}{\sin\theta}}}{\zeta k(x+\frac{s}{\sin\theta})} \tag{12}$$

Then the frequency and amplitude of the pulsed jet can be calculated

$$f=\frac{1}{T_1+T_2+T_3} \tag{13}$$

$$P_a=\rho_l c\frac{Q}{s\pi}\frac{\cos\theta}{(d_2-\frac{s}{\cos\theta})} \tag{14}$$

where f is the frequency of pulsed jet, Hz; P_a is the pressure pulsation amplitude of the pulsed jet, Pa.

3. Experiment

3.1. Experimental setup and procedure

Experiments are conducted using a specially designed setup shown in Fig. 3. The equipment consists of a high-pressure pump, valve spring blocking prototype and Brüel & Kjær dynamic pressure testing system (Type: 3560-A-002). The rock sample is cement stones mixture by quartz sand (granularity is 0.3 mm–0.6 mm and density is 3100 kg/m^3) and building cement according to cement-sand ratio 1:2.5. The uniaxial compressive strength and Poisson ratio of the rock sample are 30.6 MPa and 0.23, respectively.

Table 1
Rock breakage experimental scheme.

Group number	Stem clearance s (mm)	Upper nozzle diameter d_1 (mm)	Spring length L (mm)	Lower nozzle diameter d_2 (mm)
1	3	6	25	4
2	3	8	27	5
3	3	10	32	6
4	4	6	27	6
5	4	8	32	4
6	4	10	25	5
7	5	6	32	5
8	5	8	25	6
9	5	10	27	4
10 (contrast)	–	8	–	4

The experiments of pressure pulsation characteristics and rock breakage performances of the pulsed jet were carried out, respectively. Firstly, assembling the valve spring blocking prototype and fixing it in the shelf and adjusting its position to designed standoff distance. Secondly, starting the plunger pump and adjusting it to scheduled pressure. Thirdly, starting counting, measuring and saving the peak and valley values of instantaneous impact pressure. Finally, stopping counting and turning off the plunger pump and measuring the radius, depth and volume of the borehole forming in the rock samples.

3.2. Results analysis

3.2.1. Pressure pulsation characteristics of waterjet

The upper nozzle diameter, pre-tightening force of spring, stem clearance and lower nozzle diameter are the main structural parameters influencing the performance of the pulsed waterjet. The rock breakage depth and pressure pulsation of outlet are used as the optimization standards, and the orthogonal table $L_9(4^3)$ is chosen to conduct tests (Table 1). The pump pressure and standoff distance for these tests equal 15 MPa and 15 mm, respectively. The erosion time for each test equals one minute and each test was repeated over three times under the same conditions to assure the reliability of the experimental data. The rock breakage results of these ten structures is shown in Fig. 4. As can be seen from Fig. 4, the rock breakage effects of most pulsed jets are better than continuous jet (i.e. 10th group) and the fifth group achieves the best rock breakage depth. Fig. 5 compares the pressure changes of the 5th group and 10th group with time during experiment. The pressure fluctuation amplitude and frequency of pulsed jet modulated by the 5th prototype is larger than the continuous jet, which is the main reason for the better rock breakage effect of the 5th group. In addition, the pressure fluctuation of the continuous jet (i.e. 10th group) dues to the pressure fluctuation of the plunger pump.

The operating parameters (such as pump pressure and standoff distance) and structure parameters of the engineering prototype are quite different from the laboratory principles prototype. Thus, it is necessary to research the influences of the operating and structural parameters of the valve spring blocking tool on the jet characteristics and rock breakage

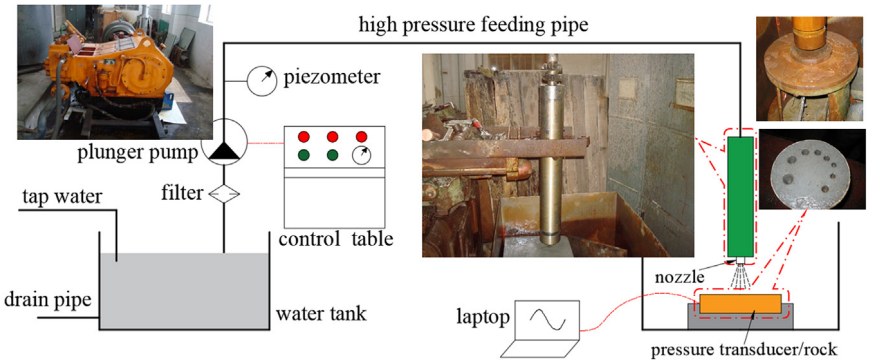

Fig. 3. Schematic diagram of the experimental setup.

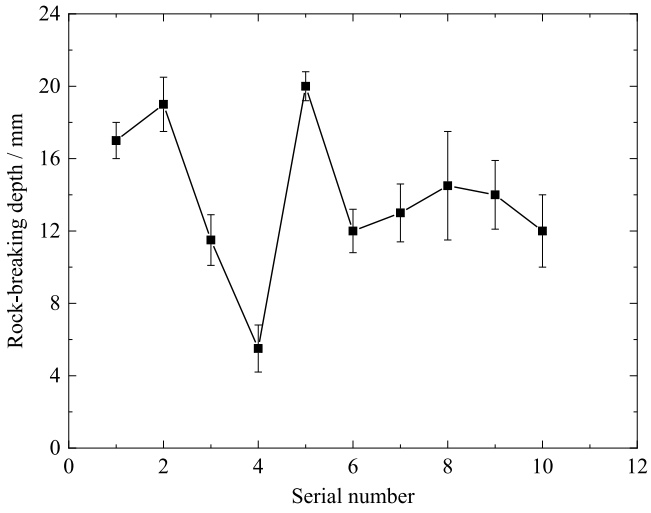

Fig. 4. Rock breakage results of structures in Table 1.

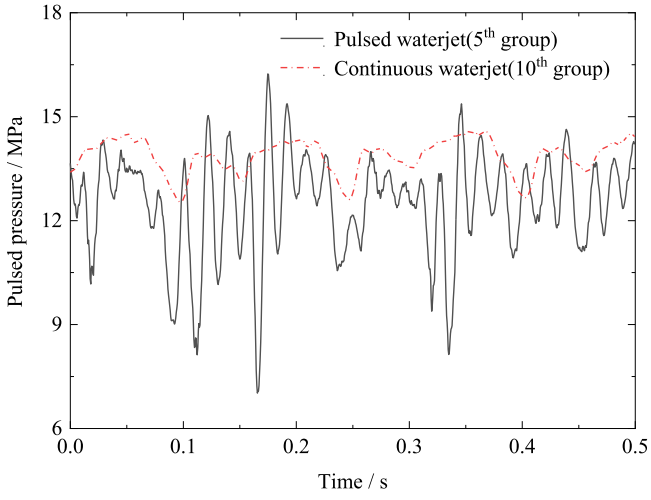

Fig. 5. Comparison of the pulsed waterjet (5th group) and continuous waterjet (10th group).

3.2.2. *Influence of operating parameters*

Choosing the 5th group prototype in Table 1 to research the influence of operating parameters (i.e. pump pressure and standoff distance) on the rock breakage effect and jet characteristics. Figs. 6 and 7 show the influence of pump pressure on the jet characteristics and rock breakage effects, respectively. As can be seen from Fig. 6, the average pressure and pressure pulsation of the pulsed jet and continuous jet both increase with increasing pump pressure. The average pressure of continuous jet is a little higher than the pulsed jet under different pump pressures. The pressure pulsation of the pulsed jet is lower than the continuous jet when the pump pressure is lower than 10 MPa and significantly higher than the continuous jet when the pump pressure is higher than 10 MPa. Corresponding to that, the rock breakage depth of these two jets are almost the same when the pump pressure is lower than 10 MPa and the rock breakage depth of the pulsed jet is significantly higher than the continuous jet when the pump pressure is higher than 10 MPa (see Fig. 7). The main reason for above phenomenon is the hydraulic energy pumped into the prototype is not enough to modulate the pulsed jet when the pump pressure is relatively small and the prototype consumes some hydraulic, which make the average pressure and pressure pulsation of pulsed jet is lower than continuous jet. When the pump pressure is higher than 10MPa and continues to increase, the prototype begins working and modulating increasingly intense pulsed jet, which results in better rock breakage effects accordingly.

Fig. 8 shows the influence of standoff distance on average pressure, pressure pulsation and rock breakage depth. From Fig. 8, the average pressure decreases slowly with increasing standoff distance and rapidly decreases when the standoff distance is higher than 27 mm. The pressure pulsation increases slowly with increasing standoff distance and rapidly increases when the standoff distance is higher than 30 mm. The reason for this phenomenon is that the jet scatters and becomes instability at the outlet when the distance is large (i.e. 30 mm), which results in low average pressure. Meanwhile, the jet center sometimes deviates from the pressure acquisition center in case of large standoff distance. All these mean the pressure data in case of large standoff distance (i.e. $>$30 mm) cannot accurately reflect the working condition inside the prototype. Different with the change of pressure, the rock breakage depth increases first and then decreases with increasing standoff distance. The rock breakage depth reaches the maximum value in case of 23 mm standoff distance. The main reason for above phenomenon is the jet is not fully expanded resulting in small impact surface, and the jet interferes with its return flow after impacting the rock sample and consumes part of the hydraulic energy when the standoff distance is relatively small. The impact surface of jet gradually unfolds and the interference with return flow decreases with increasing standoff distance, which results in better rock breakage effect. As the standoff distance continues increasing, the energy consumption of the jet before it reaching the rock sample increases sharply and the impact force weakens, which make the rock breakage depth decreasing gradually. The optimal standoff distance is 23 mm under the conditions of present experiment.

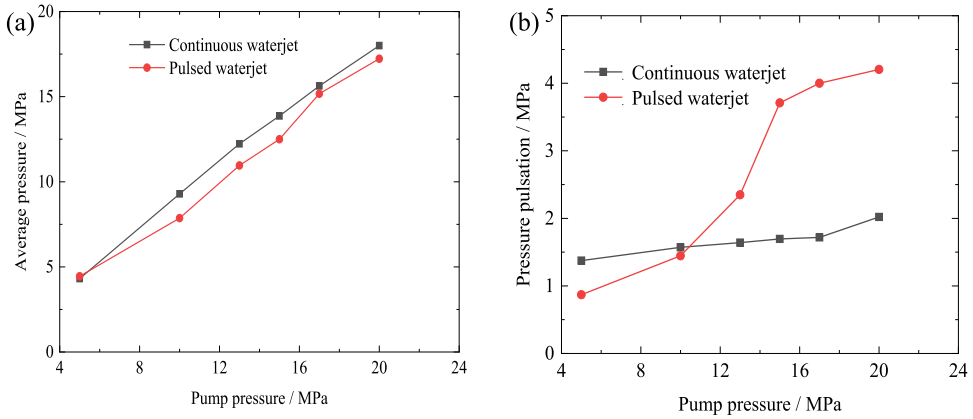

Fig. 6. Contrast of the wave of continuous jet and pulsed jet (s = 23 mm). (a) Average pressure; (b) Pressure pulsation.

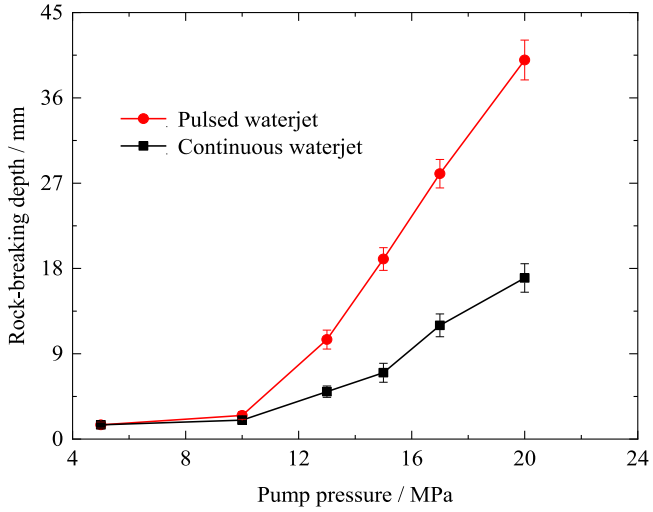

Fig. 7. Rock breakage of continuous jet and pulsed jet in different pressure (s = 23 mm).

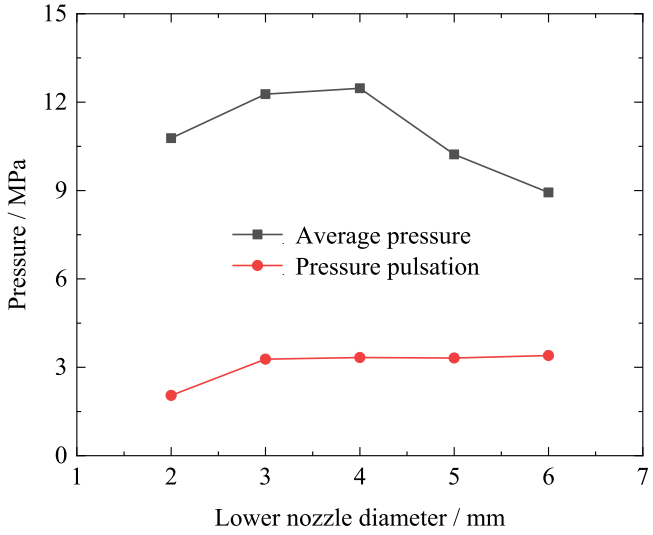

Fig. 9. Influence of lower nozzle diameter on average pressure and pressure pulsation.

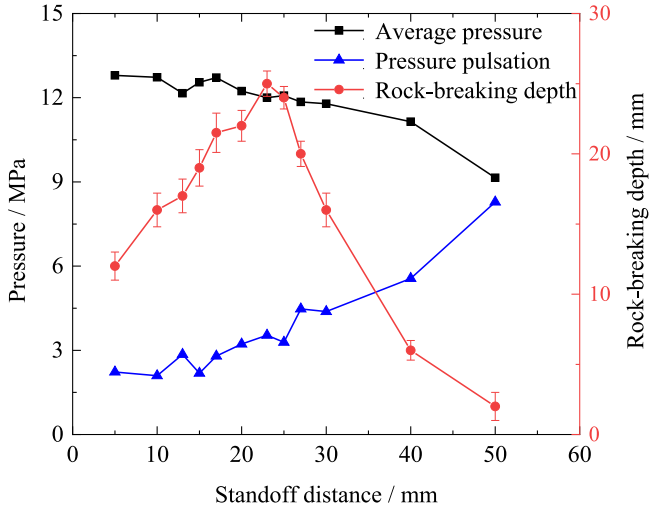

Fig. 8. Pressure and rock breakage depth of pulsed waterjet under different standoff distance (P = 15 MPa).

3.2.3. *Influence of structure parameters*

The default parameters in this section including the pump pressure P = 15 MPa, standoff distance s = 23 mm, stem clearance h = 4 mm, upper nozzle diameter d_1 = 8 mm, spring length L = 32 mm, lower nozzle diameter d_2 = 4 mm. Fig. 9 shows the influence of lower nozzle diameter on the average pressure and pressure pulsation of the pulsed jet. The average pressure of pulsed jet increases firstly and then decreases with increasing diameter of the lower nozzle and achieves the maximum when the diameter of the lower nozzle equals 4 mm. The pressure pulsation of the pulsed jet increases firstly and then enters into a plateau. From the above analysis we know that the diameter of the lower nozzle only affects the average pressure but not the pressure fluctuation of the pulsed jet. This is because the diameter of lower nozzle only affects the open area of the water but not the valve spring structure.

Fig. 10 shows the influence of upper nozzle diameter on the average pressure, pressure pulsation and rock breakage depth of the pulsed jet. The average pressure, pressure pulsation and rock breakage depth all increase firstly and then decrease with increasing diameter of the upper nozzle and achieve their maximums when the diameter of the upper nozzle equals 10 mm. The reason for this phenomenon is that the consumption of the hydraulic energy is large when the diameter of the upper

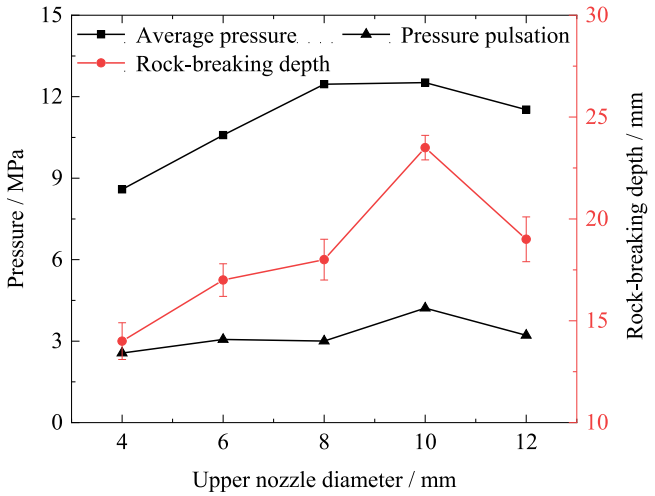

Fig. 10. Influence of upper nozzle diameter on waterjet pressure and rock breakage performance.

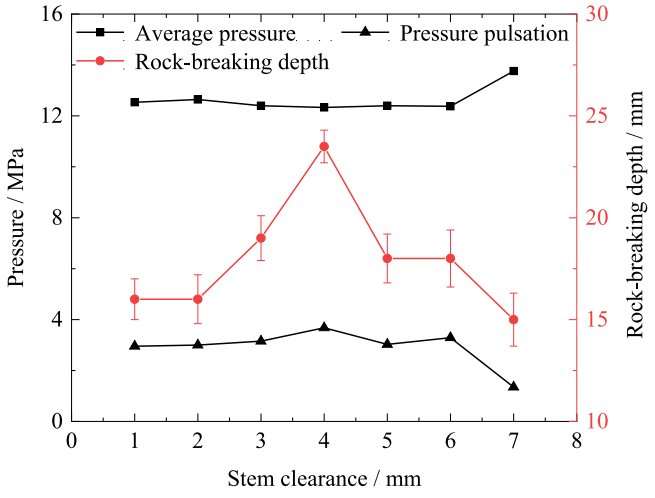

Fig. 11. Influence of stem clearance on waterjet pressure and rock breakage performance.

nozzle is relatively small and the consumption of the hydraulic energy decreases with increasing diameter of the upper nozzle. When the diameter of the upper nozzle exceeds 10 mm, the water flow velocity after it flowing through the upper nozzle is relatively small and the modulation structure cannot work effectively, which resulting in the lower rock breakage depth.

Fig. 11 shows the influence of the stem clearance on the average pressure, pressure pulsation and rock breakage depth of the pulsed jet. Results show that the average pressure of the pulsed jet keeps stable firstly and then rapidly increases, meanwhile, the pressure pulsation of the pulsed jet fluctuates firstly and then decreases rapidly. The rock breakage depth increases firstly and then decreases and achieves its maximum when the stem clearance equals 4 mm. The changes of the rock breakage depth and pressure pulsation are similar. We can infer the pressure pulsation is the main influence factor of the rock breakage depth under the conditions of similar average pressure.

Fig. 12 shows the influence of spring length on the average pressure, pressure pulsation and rock breakage depth of the pulsed jet. The spring length determines the preload of the spring

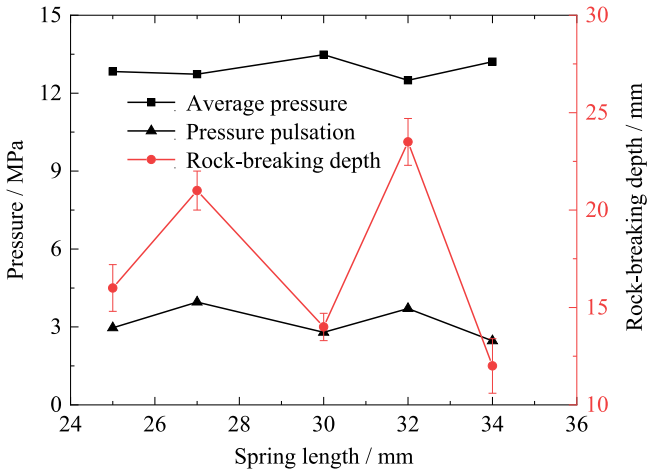

Fig. 12. Influence of spring length on waterjet pressure and rock breakage performance.

and the preload directly affects the working frequency of the modulation tool and the performance of the pulse jet. As can be seen from Fig. 12, the average pressure and pressure pulsation fluctuates slightly while the rock breakage depth fluctuates sharply. The rock breakage depth reaches to maximum when the spring length equals 32 mm.

Previous single factor experiments suggest that the diameter of the lower nozzle only affects the average pressure but not the pressure fluctuation of the pulsed jet. However, the other structural parameters will interact with each other, including the diameter of upper nozzle d_1, spring length L and stem clearance s. The pressure pulsation and rock breakage depth of the pulsed jet are chosen as the optimization standards, and the twenty-seven group orthogonal tests are conducted (see Table 2). The pump pressure and standoff distance are respectively 15 MPa and 23 mm during all the tests. Fig. 13 shows the average pressure, pressure pulsation and rock breakage depth of the pulsed jets under different structural parameters in Table 2. The average pressure of the pulsed jet is relatively gentle, ranging from 10 MPa to 14 MPa. The pressure pulsation fluctuates greatly and has no obvious rule, among which the pressure pulsations of groups three, fifteen and eighteen are relatively larger. The rock breakage depths also fluctuate greatly and the changing trends of its middle part are similar to the pressure pulsation, among which the rock breakage depth of groups nine, fifteen and eighteen are relatively larger. Comparing the results of the average pressure, pressure pulsation and rock breakage depth, we can see that group eighteen is the optimal structure. Fig. 14 shows the theoretical frequencies calculated by Eq. (13) with experimental values. The calculating parameters include the inner cylinder length 0.38 m, the spring stiffness $k = 15100$ N/m, the stem mass $m = 0.95$ kg, the displacement of pump $Q = 3$ L/s, the density of water $\rho_l = 1000$ kg/m^3 and the propagation velocity of pressure wave $c = 1400$ m/s. From Fig. 14 we can see that the change of the theoretical frequencies is consistent with the experimental values. Meanwhile, the theoretical frequencies are slightly higher than the experimental values, which dues to the ignorance of friction resistance of some components and viscous resistance of fluid or the limitation of testing conditions. The error between the theoretical and experimental results of frequencies is ranging from 0.3% to 22.1%, which is within the allowable range of its engineering application.

Table 2
The result of rock breakage experiment and the dynamic pressure test.

Group number	Diameter of upper nozzle d_1 (mm)	Spring length L (mm)	Stem clearance s (mm)
1	6	25	3
2	6	25	4
3	6	25	5
4	6	27	3
5	6	27	4
6	6	27	5
7	6	32	3
8	6	32	4
9	6	32	5
10	8	25	3
11	8	25	4
12	8	25	5
13	8	27	3
14	8	27	4
15	8	27	5
16	8	32	3
17	8	32	4
18	8	32	5
19	10	25	3
20	10	25	4
21	10	25	5
22	10	27	3
23	10	27	4
24	10	27	5
25	10	32	3
26	10	32	4
27	10	32	5

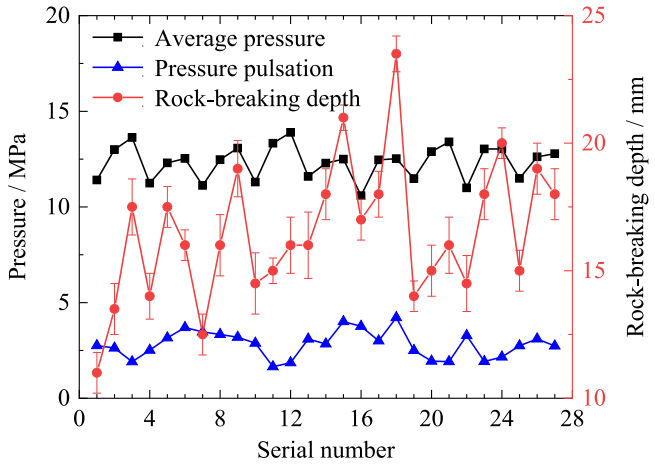

Fig. 13. The orthogonal test pressure and rock breakage results.

4. Conclusions

A novel valve spring blocking drilling tool for modulating pulsed jet was proposed in this paper. The pressure pulsation characteristics and rock breakage performances of the pulsed jet were studied by theoretical calculation and experiments. The main results of the present study are described as follows:

(1) The designed valve spring blocking tool can effectively modulate pulsed jet through the reciprocating motion of the stem under the pressure difference.

(2) The theoretical frequencies are slightly higher than the experimental values, which dues to the ignorance of friction resistance of some components and viscous resistance of fluid and the error is ranging from 0.3% to 22.1%, which is within the allowable range of its engineering applications.

(3) The diameter of the lower nozzle only affects the average pressure but not the pressure fluctuation of the pulsed jet, while the upper nozzle diameter, spring length and stem clearance will affect its pressure pulsation and rock breakage performance. The optimal structure parameters for the prototype are as follows: the upper nozzle diameter $d_1 = 10$ mm, the spring length $L = 32$ mm, stem clearance $s = 4$ mm and the lower nozzle diameter $d_2 = 4$ mm.

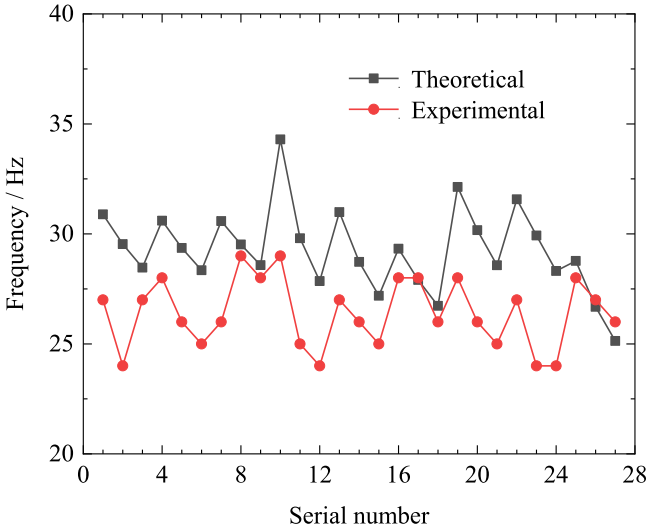

Fig. 14. The frequency result of theory and experiment.

Declaration of competing interest

The authors declare that they have no known competing financial interests or personal relationships that could have appeared to influence the work reported in this paper.

CRediT authorship contribution statement

Peng Wang: Conceptualization, Methodology. **Zhina Li:** Writing - original draft. **Hongjian Ni:** Supervision. **Yuandong Liu:** Writing - review & editing. **Peng Dou:** Visualization, Investigation.

Acknowledgments

The authors gratefully acknowledge the financial support of the National Natural Science Foundation of China (Grant No. 51704323), the Fundamental Research Funds for the Central Universities, China (Grant No. 18CX02009A, 18CX02177A), and Qingdao headstream innovation and applied basic research project, China (Grant No. 19-6-2-22-cg). The authors express their appreciation for the comments of the anonymous reviewers and the editors.

References

Bizanti, 1990. Jet pulsing may allow better hole cleaning. Oil Gas J. - OIL GAS J. 88, 67–68.

Bowden, F.P., Field, J.E., 1964. The brittle fracture of solids by liquid impact, by solid impact, and by shock. Proc. R. Soc. Lond. Ser. A Math. Phys. Sci. 282, 331–352.

Dehkhoda, S., Hood, M., 2014. The internal failure of rock samples subjected to pulsed water jet impacts. Int. J. Rock Mech. Min. Sci. 66, 91–96.

Dehkhoda, S., Hood, M., Alehossein, H., Buttsworth, D., 2012. Analytical and experimental study of pressure dynamics in a pulsed water jet device. Flow Turbul. Combust. 89, 97–119.

Farmer, I.W., Attewell, P.B., 1965. Rock penetration by high velocity water jet: A review of the general problem and an experimental study. Int. J. Rock Mech. Min. Sci. Geomech. Abstr. 2, 135–153.

Foldyna, J., Heiniger, K., Mettler, S., Sitek, L., Scucka, J., 2020. Enhancing of water jet effects by pulsations Zlepšenie účinku vodného lúča pulzáciou.
Foldyna, J., Sitek, L., Habán, V., 2006. Acoustic wave propagation in high-pressure system. Ultrasonics 44, 1457–1460.
Foldyna, J., Sitek, L., Ščučka, J., Martinec, P., Valíček, J., Páleníková, K., 2009. Effects of pulsating water jet impact on aluminium surface. J. Mater Process. Technol. 209, 6174–6180.
Foldyna, J., Sitek, L., Švehla, B., Švehla, Š., 2004. Utilization of ultrasound to enhance high-speed water jet effects. Ultrason. Sonochem. 11, 131–137.
Ghadi, S., Esmailpour, K., Hosseinalipour, S.M., Mujumdar, A., 2016. Experimental study of formation and development of coherent vortical structures in pulsed turbulent impinging jet. Exp. Therm Fluid Sci. 74, 382–389.
Heymann, F., 1970. High-speed impact between a liquid drop and a solid surface. J. Appl. Phys. 40, 5113–5122.
Hood, M., Nordlund, R., Thimons, E., 1990. A study of rock erosion using high-pressure water jets. Int. J. Rock Mech. Min. Sci. Geomech. Abstr. 27, 77–86.
Johnson, V.E., Conn, A.F., Lindenmuth, W.T., Chahine, G., Frederick, G.S., 1982. Self-resonating cavitating jets. In: 6th International Symposium on Jet Cutting Technology.
Lesser, M.B., Field, J.E., 2003. The impact of compressible liquids. Annu. Rev. Fluid Mech. 15, 97–122.
Li, D., Kang, Y., Ding, X., Wang, X., Fang, Z., 2016. Effects of area discontinuity at nozzle inlet on the characteristics of high speed self-excited oscillation pulsed waterjets. Exp. Therm Fluid Sci. 79, 254–265.
Liu, W., Kang, Y., Zhang, M., Wang, X., Li, D., Xie, L., 2018. Experimental and theoretical analysis on chamber pressure of a self-resonating cavitation waterjet. Ocean Eng. 151, 33–45.
Liu, Y., Wei, J., Ren, T., Lu, Z., 2015. Experimental study of flow field structure of interrupted pulsed water jet and breakage of hard rock. Int. J. Rock Mech. Min. Sci. 78, 253–261.
Liu, Y., Zhang, J., Wei, J., Liu, X., 2020. Optimum structure of a laval nozzle for an abrasive air jet based on nozzle pressure ratio. Powder Technol. 364, 343–362.
Lu, Y., Huang, F., Liu, X., Ao, X., 2015. On the failure pattern of sandstone impacted by high-velocity water jet. Int. J. Impact Eng. 76, 67–74.
Momber, A.W., 2003. An SEM-study of high-speed hydrodynamic erosion of cementitious composites. Composites B 34, 135–142.
Morel, T., 1979. Experimental study of a jet-driven Helmholtz oscillator. J. Fluids Eng. 101, 383–390.
Nebeker, E.B., 1987. Percussive jets - state-of-the-art. In: Proc. of the 4th U.S. Water Jet Symposium.
Rein, M., 1993. Phenomena of liquid drop impact on solid and liquid surfaces. Fluid Dyn. Res. 12, 61–93.
Riha, Z., Foldyna, J., 2012. Ultrasonic pulsations of pressure in a water jet cutting tool. Tehnicki Vjesnik 19, 487–491.
Sahaya Grinspan, A., Gnanamoorthy, R., 2010. Impact force of low velocity liquid droplets measured using piezoelectric PVDF film. Colloids Surf. A 356, 162–168.
Vijaym, M.M., 1995. Power of pulsed liquid jets. Int. J. Rock Mech. Min. Sci. Geomech. Abstr. 32 (2), A84.
Xue, Q., Leung, H., Huang, L., Zhang, R., Liu, B., Wang, J., Li, L., 2019. Modeling of torsional oscillation of drillstring dynamics. Nonlinear Dynam. 96, 267–283.